ORIGINAL ARTICLE

Journal Section

Finite Element Modeling with Subject-specific Mechanical Properties to Assess Knee Osteoarthritis Initiation and Progression

Nathan Lampen[1] | **Haoyun Su**[1] | **Deva D. Chan PhD**[2] | **Pingkun Yan PhD**[1]

[1]Biomedical Engineering, Rensselaer Polytechnic Institute, Troy, New York, 12180, U.S.

[2]Weldon School of Biomedical Engineering, Purdue University, West Lafayette, Indiana, 47907, U.S.

Correspondence
Deva D. Chan & Pingkun Yan
Email: chand@purdue.edu, yanp2@rpi.edu

Funding information
National Science Foundation, Grant No. 1944394 (DDC)

Finite element models of the knee are useful for investigating regional cartilage mechanics in studies of osteoarthritis. Models of the knee often implement joint geometry obtained from MRI or gait kinematics from motion capture to increase model specificity for a given subject. However, previous works ignore the differences in cartilage material properties that exist regionally and from patient to patient. This paper presents a method to create subject-specific finite element models of the knee that assigns cartilage material properties from T_2 relaxometry. We compared our T_2-refined model to identical models with homogeneous material properties. When tested on three subjects from the Osteoarthritis Initiative dataset, we found the T_2-refined models estimated higher principal stresses and shear strains in most cartilage regions as compared to their corresponding homogeneous material models. Measures of cumulative stress within regions of a T_2-refined model also correlated better with the region's MRI Osteoarthritis Knee Score as compared to the homogeneous model. We conclude that spatially heterogeneous T_2-refined material properties improve the patient-specificity of finite element models compared to homogeneous material properties in osteoarthritis progression studies.

KEYWORDS
osteoarthritis, finite element model, cartilage, material properties, magnetic resonance imaging

Abbreviations: MRI, Magnetic Resonance Imaging; OA, Osteoarthritis; FE, Finite Element; MOAKS; MRI Osteoarthritis Knee Score;

1 | INTRODUCTION

Osteoarthritis (OA) of the knee is a painful and debilitating disease characterized by degeneration of articular cartilage [1]. Cartilage loss results from changes in the extracellular matrix, most notably the loss of proteoglycan and collagen content, which alters the tissue's mechanical properties [2]. An OA diagnosis can be confirmed with evidence of morphological changes, such as joint space narrowing and osteophytes, that are typically seen in X-ray imaging. However, significant cartilage degeneration can occur long before joint space narrowing or osteophytes are visible in plain X-ray images [3]. Several studies have even observed poor correlation between cartilage degeneration and the radiographic features used to diagnose OA [4, 5, 6, 7]. The insensitivity of radiography to identify early OA changes is a barrier to timely implementation of non-operative treatments. These nonoperative treatments may include established methods such as weight loss, muscle strengthening, pain relievers, and nonsteroidal anti-inflammatory drugs, but also newer methods such as hyaluronic acid, corticosteroid, platelet-rich plasma, and stem cell treatments [8]. Predictive modeling of osteoarthritis progression is a growing field of research that aims to decrease the time to diagnosis [9, 10]. Since OA progression varies greatly from patient to patient, predictive models should be customized to a subject's unique morphology and material properties. Finite element (FE) modeling is a well-established approach for creating predictive models with subject-specific geometry and material properties.

FE models have been used to analyze tissue loading, estimate stress, and predict regions at increased risk of mechanical failure due to OA progression in a subject-specific way [11, 12]. Current FE modeling approaches use joint geometry, joint kinematics, or estimated joint reaction forces to create more subject-specific models. Joint geometry can be obtained through imaging and subsequent segmentation of tissues [13, 12]. Joint kinematics, such as from video motion capture of the gait cycle, can be implemented to approximate *in vivo* boundary conditions [14]. While geometry and motion are readily measurable parameters, determining subject-specific, *in vivo* tissue material properties to remains a challenge.

Magnetic resonance imaging (MRI) can be used to estimate the matrix constituents and material properties of articular cartilage [15, 16, 17, 18, 19, 20]. Since T_2 MRI captures several factors essential to the macromolecular framework of cartilage, including changes in proteoglycan and collagen content, it is also correlated with the mechanical properties of the tissue [21]. Previous work has shown that FE models with collagen fibril orientation refined by T_2 relaxation or diffusion tensor MRI produce significantly different predictions of maximum principal stresses than models with collagen fibril orientation obtained from literature [22, 23, 24]. We therefore hypothesize that a subject-specific FE model with element-wise material properties informed by T_2 relaxation time will produce significantly different levels of stress and strain, enhance model sensitivity to localized stress and strain, and thus improve prediction of regions with an increased risk of tissue degeneration as compared to an FE model with homogeneous material properties. In this paper, we developed a method for refining material properties from T_2 relaxometry to improve the patient-specificity of FE models of the knee.

2 | METHODS

2.1 | Data

This study used imaging data from the Osteoarthritis Initiative (OAI), a publicly available dataset for OA research. OAI (`https://nda.nih.gov/oai/`) is a multicenter, ten-year observational study investigating knee OA in 4,796 subjects in the United States. The OAI includes three cohorts: a progression cohort displaying symptomatic knee OA at the baseline examination, an incidence cohort not displaying OA but at an increased risk of developing OA at baseline, and a control cohort with no display or risk of developing OA at baseline. For this study, we selected imaging data from one subject in the progression cohort and two subjects

TABLE 1 Subject information

Subject	OAI Subject ID	Sex	Age at Baseline	Race	Subcohort[a]	KL at Baseline[b]	MOAKS[c]
1	9932809	F	66	Asian	1	2	Baseline only
2	9948792	M	64	White	2	0	NA
3	9988421	F	54	Black	2	0	All timepoints

[a] The OAI separates patients into three cohorts: (1) a progression cohort displaying symptomatic knee OA at the baseline examination, (2) an incidence cohort not displaying OA but at an increased risk of developing OA at baseline, and (3) a control cohort with no display or risk of developing OA at baseline.

[b] Kellgren-Lawrence (KL) grade was determined by a radiologist at the baseline imaging timepoint. Simply put, the Kellgren-Lawrence classes are as follows: (0) absence of OA, (1) doubtful OA, (2) minimal OA, (3) moderate OA, and (4) severe OA.

[c] Availability of MRI Osteoarthritis Knee Score (MOAKS) for the given patient. MOAKS is regional a semi-quantitative scoring assessment which ranks the degree of cartilage loss.

in the incidence cohort. The selected subjects were a mix of male and female, from three different racial groups, and with ages ranging from 54 to 66 at the time of baseline imaging (Table 1). Right knee images at the baseline time point were used for all three subjects. At the time of imaging, subject 1 was classified as Kellgren-Lawrence (KL) grade 2, which is considered to be minimal OA, and subjects 2 and 3 were classified as KL grade 0, which is no sign of OA. A subject with KL grade 2 OA was chosen to test model sensitivity to early OA since changes to the extra-cellular matrix would likely have occurred by this stage without major loss of cartilage tissue volume [25]. OA progression was evaluated with the MRI Osteoarthritis Knee Score (MOAKS) score [26] at multiple time points for subject 3 through the Pivotal OAI MR Imaging Analysis study [27, 28]. MOAKS are assigned based on the percent of cartilage loss observed in a given region, where grade 0 indicates no loss, grade 1 indicates $< 10\%$ loss, grade 2 indicates $10 - 75\%$ loss, and grade 3 indicates $> 75\%$ loss.

MR images of the knees from OAI were obtained using a Siemens Trio 3.0 T scanner with quadrature transmit-receive coils (USA Instruments, Aurora, OH, USA) [29]. The scan protocol included the following sequences: (1) sagittal 3-D dual echo in the steady state (DESS) with selective water excitation TE = 4.7 ms, TR = 16.3 ms, flip angle = 25° and (2) sagittal T_2-Map, TE = 10, 20, 30, 40, 50, 60, 70 ms, TR = 2700.

FE meshes of cartilage and menisci for the selected subjects were obtained courtesy of David Pierce [30]. Segmentation of cartilage and menisci for the selected subjects were performed on 3D DESS MRI, and FE meshes were constructed using solid, 8-node trilinear hexahedral elements [30] for FE analysis in FEBio Studio version 1.5.0 [31] as detailed in the following paragraphs .

2.2 | Model Overview

Our modeling workflow is shown in Fig. 1, as initially proposed in [32]. Briefly, the T_2 map is filtered for the subject of interest (Fig. 1A). Next, all regions of articular cartilage are selected from the T_2 map (Fig. 1B). Material properties within a subject-specific finite element mesh are then calculated from the segmented T_2 map (Fig. 1C). Finally, a simple gait cycle is simulated and key measures of stress and strain are computed for model evaluation (Fig. 1D). In the following sections, we describe each of these steps in depth.

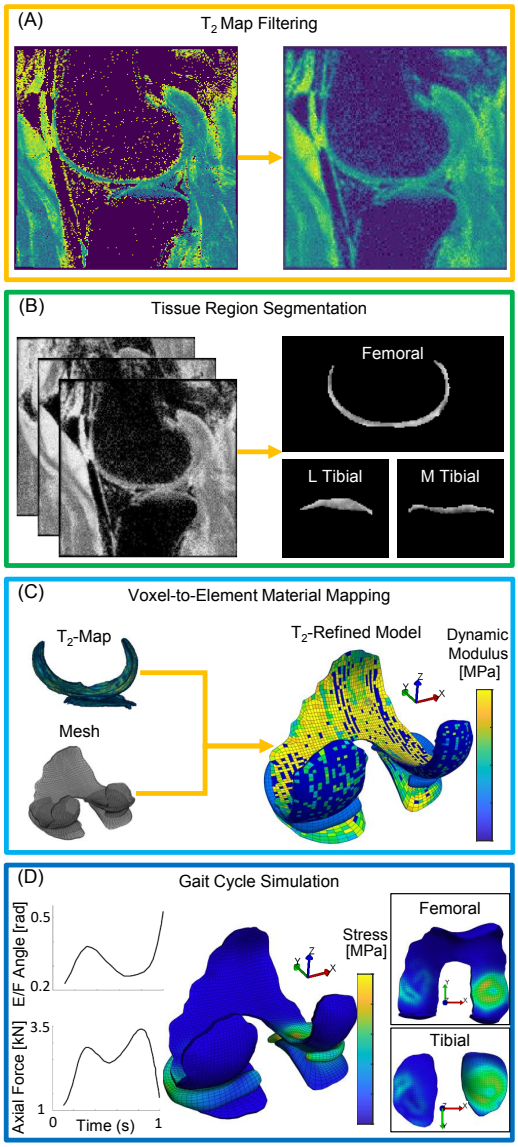

FIGURE 1 Overview of the developed T_2-refined material model analysis.

2.3 | Preprocessing T_2 Maps

We used T_2 maps as an input to the model. T_2 maps were filtered using a gradient anisotropic diffusion filter from SimpleITK[1] with 5 iterations, timestep = 0.125, and conductance = 3. Filtering was performed in the T_2 maps to smooth changes in T_2 value between adjacent pixels (Fig. 1A). Filtering reduces the likelihood of large differences in material properties between adjacent elements in later modeling steps. Upper and lower T_2 thresholds (> 70 ms and < 10 ms) were also implemented to eliminate values that were outside the range of T_2 echo times.

2.4 | Mapping T_2 Relaxation Times to Material Properties

The material properties of the subject-specific FE models, which included all articular cartilage and meniscus regions, were customized using a custom built voxel-to-element mapping method created in MATLAB version R2020a (MathWorks, Natick, MA) [33]. Articular cartilage and menisci were both modeled as Neo-Hookean materials due to the relative equivalence of biphasic and elastic materials during short-time responses [34]. While many other FE studies model articular cartilage and menisci as either anisotropic or transversely isotropic materials, we chose to assume isotropy to simplify the model since the focus of this work is to understand the impact of refining materials based on T_2 imaging. For each model, the T_2 map was first registered with the corresponding fixed 3D DESS MRI image. Segmentation masks from the 3D DESS image [30] were then overlaid to select cartilage regions within the T_2 map (Fig. 1B). The images containing the segmented cartilage and meniscus regions were converted to the same global coordinate system used by the FE mesh. Next, the TransformPhysicalPointToIndex function from SimpleITK[1] was used to match the T_2 voxels to elements in the FE model (Fig. 1C). In this process, the function used the centroid coordinates of each element in the FE model to search for the corre-

[1] https://simpleitk.org

sponding voxel in the segmented T_2 map. The function returned the index of the matching voxel, which was used to find the voxel's T_2 relaxation value. The voxel relaxation values were then used to determine the dynamic modulus of the respective elements [21].

$$E_D = (-3.5/3 \times 10^5)T + 9.75 \times 10^6 \quad (1)$$

Equation (1) was used to calculate the dynamic modulus (E_D) in [Pa] from T_2 time (T) in [ms]. The number of unique materials desired was also included as an input to the model.

$$W = \frac{T_U - T_L}{N} \quad (2)$$

Voxels were binned according to equation (2), where (W) is the bin width, (T_U) is the upper T_2 limit, (T_L) is the lower T_2 limit, and (N) is the number of unique materials. All voxels within a defined bin were converted to the same E_D value to decrease the number of distinct materials, reducing model complexity. The number of materials (N) could be varied at will. In addition, defining N = 1 would be equivalent to a model with homogeneous material properties. Increasing the number of materials may provide a higher degree of sensitivity to localized changes in modulus, but at the expense of increasing model complexity and computation time. Table 2 shows the material properties used for the cartilage and menisci in the T_2-refined and homogeneous material models. The upper and lower limit for the dynamic modulus were chosen based on the range of dynamic modulus seen in cartilage with varying levels of degradation [35]. For all T_2-refined models presented the number of materials was set to 10 through an empirical study. We updated our method to use dynamic modulus instead of elastic modulus, which was presented in our previous work [32]. The dynamic modulus was chosen instead of elastic modulus since the testing protocol used by [21] to determine dynamic modulus was closest to the loading regimen of the stance phase of a typical gait cycle used in our simulation. In the aforementioned study, the equilibrium response elastic (Young's) modulus was measured using the stress-relaxation method, whereas dynamic modulus was measured using 1 Hz sinusoidal loading [21].

TABLE 2 Material properties used in FE models

Model	Homogeneous		T_2-refined	
Tissue	Cart	Men	Cart	Men
E_D, MPa	5	20[a]	1-8[b]	20
ν	0.45[c]	0.3[a]	0.45	0.3

Abbreviations: Cart, cartilage; Men, menisci; E_D, dynamic modulus; ν, Poisson's ratio

a (Mononen et al., 2015 [14])

b Range of dynamic modulus (Nissi et al., 2007 [21]; Waldstein et al., 2016 [35])

c (Klets et al., 2016 [36])

2.5 | FE Mechanical Simulation

Mechanical simulations were performed in FEBio Studio version 1.5.0 [31]. The FE models with customized material properties were exported from MATLAB to files compatible with FEBio using the Geometry and Image-Based Bioengineering add-On (GIBBON) MATLAB toolbox [37]. Since moderate activity (e.g. walking) comprises around 30% of daily activity [38], we applied average motion and loading from the stance phase of a walking gait cycle [39]. A simplified gait cycle with transient loading (≈[1000,3500](N)) and knee extension-flexion angle (≈[0.2,0.5](rad)) was assigned to the models as time-dependent boundary conditions [39], as shown in Fig. 1D. The gate loading acted along an axis defined through a reference point in the middle of the femoral epicondyles parallel to the tibial-diaphyseal axis in the $-z$ direction. The proximal surface of the femoral cartilage was fixed to the reference point using a rigid interface contact and all nodes on the distal surface of the medial and lateral tibial cartilage were fixed [14]. The mensici were constrained using a fixed displacement boundary condition applied to the meniscal horns where the meniscal roots would

TABLE 3 Parameters used in sensitivity study

Variable	-50%	-25%	Ref	+25%	+50%
E_D, MPa	-	1-6	1-8	1-10	1-12
Variable	-20%	-10%	Ref	+10%	+20%
N	8	9	10	11	12

Abbreviations: E_D, dynamic modulus; N, number of materials

typically attach [40, 41]. Before the stance phase commenced, models underwent a 0.1 second ramping stage, which adjusted the model to match the initial placement and force at the beginning of the stance phase. The stance phase lasted 0.9 seconds. Two models were built for each subject of interest: (i) a model with voxel-to-element T_2-refined E_D and (ii) a model with homogeneous E_D. Both models used the same subject-specific mesh, boundary conditions, contact definitions, and rigid constraints, enabling a more direct comparison of the effect of T_2-refinement of material properties.

2.6 | Comparison of T_2-refined and Homogeneous Material Models

The T_2-refined and homogeneous model simulation results were compared by investigating the maximum and minimum principal stresses and strains, as well as and maximum shear stress and strain within all regions of articular cartilage. The cartilage regions were defined consistent to the MOAKS evaluation [26], where the femoral and tibial cartilage are divided into medial and lateral halves, then further into anterior, central, and posterior sections. Previous studies have assumed maximum principal stresses exceeding 7 MPa to trigger degeneration of collagen, while strains above 30% trigger proteoglycan degeneration within articular cartilage [42, 43]. The cumulative maximum principal stress was also calculated for each element as described by Klets et al. [44]. The total number of elements within a region that exceeded a maximum cumulative stress threshold of 0.5 MPa were calculated for the T_2-refined and homogeneous models. A correlation between the number of elements exceeding the cumulative stress threshold within a given region and the region's MOAKS score was investigated for patient 3 (since regional MOAKS scores were only available for patient 3).

Statistical analysis was performed in MATLAB version R2020a (MathWorks, Natick, MA) [33]. The normality of regional stress and strain measures were evaluated using a Shapiro-Wilk test [45]. The Wilcoxon signed-rank test was used to test for significant differences between regional measures from the T_2-refined and homogeneous material models. Spearman's rank correlation was used to investigate correlation between the maximum cumulative stress and MOAKS score within a given region. For all statistical tests, the level of significance was $p < 0.05$.

A sensitivity study was used to investigate the effect of changing the number of materials (N) and the upper limit of the dynamic modulus in a T_2-refined material model. Table 3 shows the range of values tested for each variable. The ranges chosen for E_D were based on the experimental data obtained by [35].

3 | RESULTS

The T_2-refined model simulations displayed higher levels of stress and strain and also demonstrated better spatial detail as compared to the homogeneous models, suggesting an improved ability to pinpoint locations with elevated stress and strain levels (Fig. 2). The T_2-refined material models showed significantly higher maximum 1st principal stress, shear strain, and cumulative stress in most cartilage regions as compared to the homogeneous models for all subjects. The difference between the T_2-refined and homogeneous models was most prominently seen in the increase in predicted maximum shear strain (Fig. 3). The maximum principal stress threshold of 5 MPa for collagen degeneration as defined by [42] was not exceeded in the cartilage for any subjects, although principal stresses

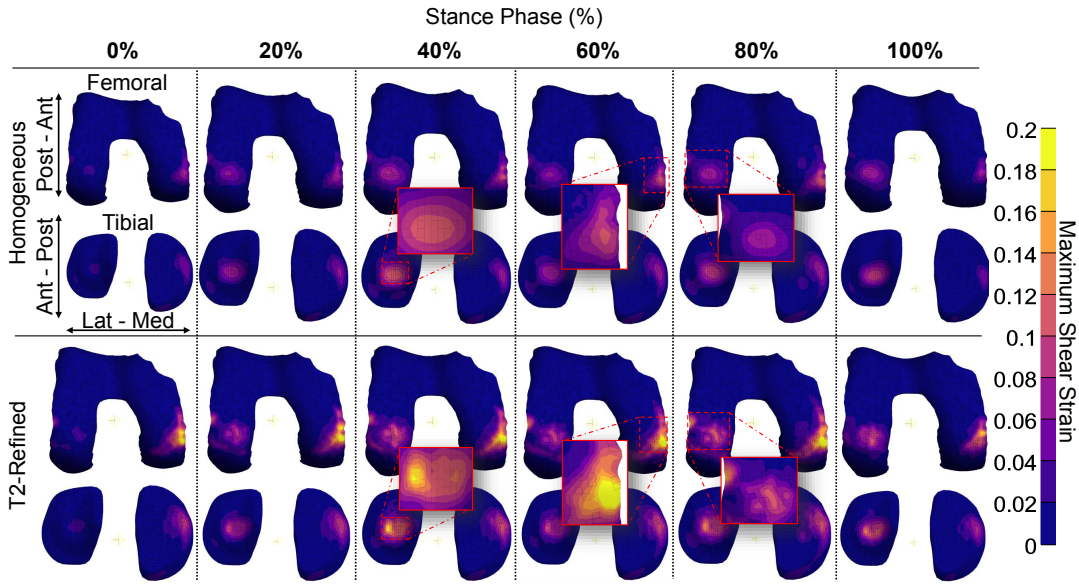

FIGURE 2 The simulation results for patient 1 showed higher shear strains in the T_2-refined model as compared to the homogeneous model for the same patient. The T_2-refined model also showed much higher spatial detail in regions with elevated shear strain levels, as seen in the magnified regions.

above 5 MPa were observed in the meniscus. The shear strain threshold of 0.3 for proteoglycan degeneration defined by [43] was exceeded in several regions of the cartilage for all three subjects.

Significant correlation was seen between the number of elements exceeding the 0.5 MPa cumulative stress threshold and the regional MOAKS scores in the T_2-refined model but not in the homogeneous model (Fig. 4). The T_2-refined model had significant correlation both at the baseline time point and at the end-of-study time point.

In the sensitivity study of the dynamic modulus range, when the upper limit was set to 6 MPa (a 25% decrease) the maximum shear strain increased by nearly 40% in the first half of the gait cycle as compared to the reference 8 MPa modulus limit (Figure 6). In comparison, decreasing number of materials by 20% only caused about a 10% decrease in the maximum shear strain (Figure 7).

4 | DISCUSSION

In this study, we developed a subject-specific FE model that implements T_2 mapping with MRI to assign spatially heterogeneous dynamic moduli to cartilage finite elements, using a custom voxel-to-element pipeline. Current radiographic evaluation of OA is not sensitive to changes seen in early OA resulting in delayed diagnosis. Predictive models of OA may reduce the time to diagnosis, but since OA progression varies greatly from patient to patient, they need to be customized to a given subject. FE models can be used to understand cartilage loading and predict degeneration in a subject-specific manner. Many previous FE studies of the knee utilize imaged joint geometry or motion captured gait cycle loading to create subject-specific FE models [46, 43, 11, 9, 47]. A study by Räsänen et al. used sodium MRI to determine localized fixed charge density in subject-specific models of cartilage loading[24]. Other recent FE models have implemented algorithms to model fixed charged density loss and compare it to

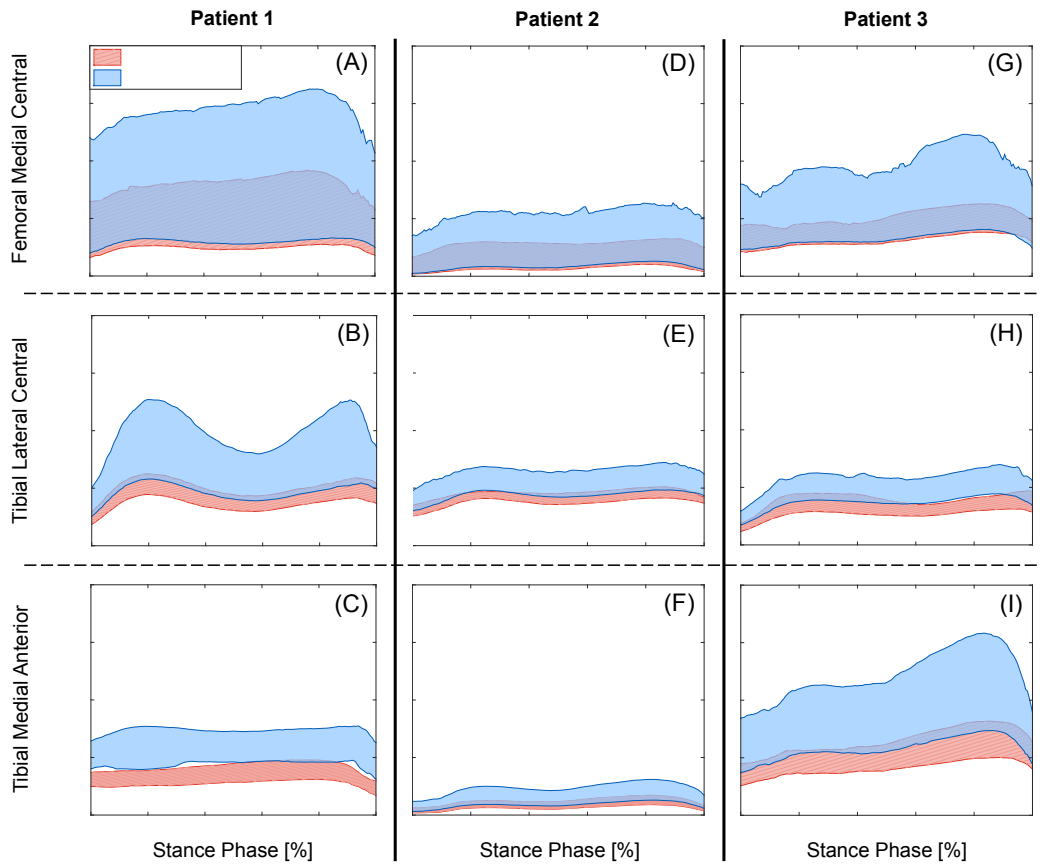

FIGURE 3 Representative regions from each patient showing elevated maximum shear strain. The femoral cartilage was broken into medial, and lateral halves, then further subdivided into anterior, central, and posterior sections. Maximum shear strain was consistently higher in the T_2-refined model (blue solid region) than in the Homogeneous model (red hatched region) in most regions throughout the cartilage. In a few cases, the shear strain levels estimated by the T_2-refined model exceeded the 30% strain threshold linked with proteoglycan loss while the Homogeneous model did not (A,I).

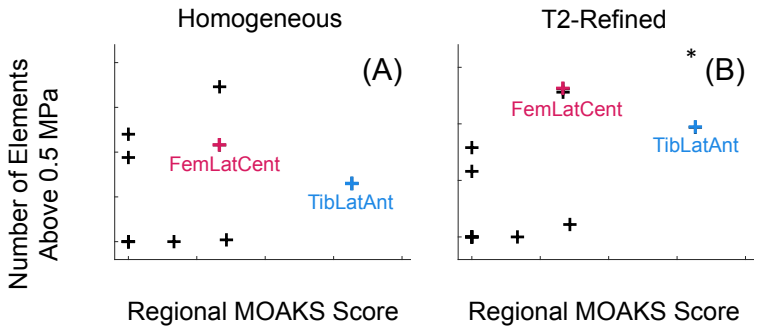

FIGURE 4 The T_2-refined model improved correlation with regional MOAKS scores at the end-of-study imaging timepoint for patient 3. Spearman rank correlation between the number of elements exceeding 0.5 MPa within a given region and the region's MOAKS score was used as the measure of correlation. Significance was set to $p<0.05$. The femoral lateral central (FemLatCent) and tibial lateral anterior (TibLatAnt) regions showed the most change between the homogeneous (A) and T_2-refined (B) models. The stress magnitude of these regions is shown in figure 5

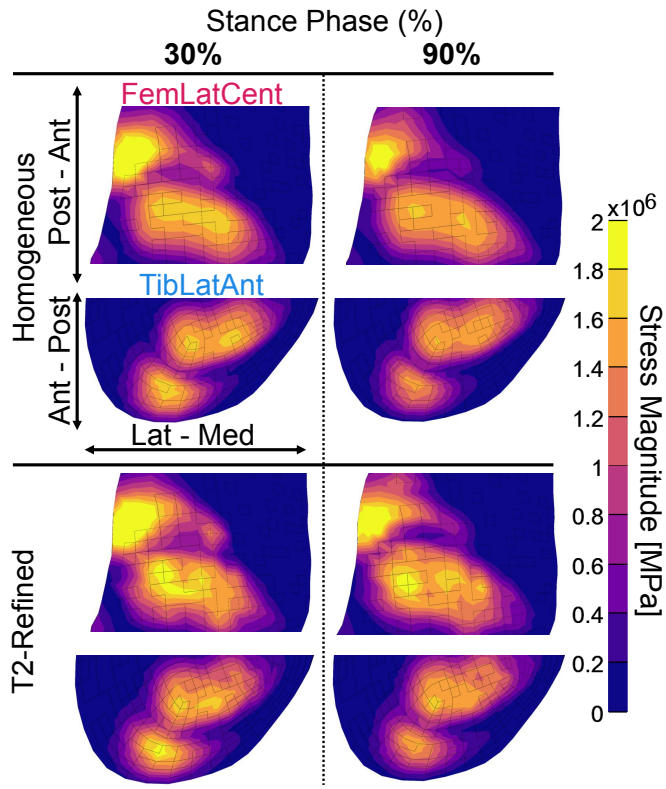

FIGURE 5 The regions with the most change in cumulative stress were the femoral lateral central (FemLatCent) and tibial lateral anterior (TibLatAnt) regions. The stress magnitude at two timepoints within the gait cycle are shown to illustrate the difference between the two material models. The T_2-refined model showed elevated stress levels in these regions.

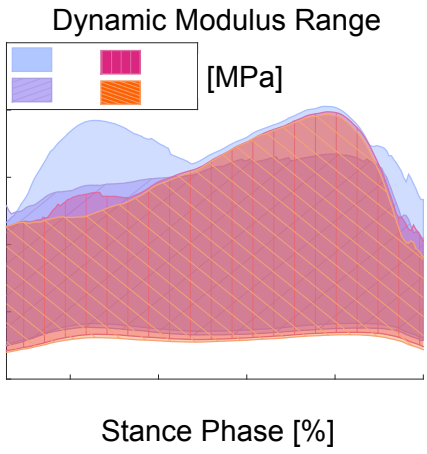

FIGURE 6 A sensitivity study of the range of the dynamic modulus in the T_2-refined material model showed that lowering the upper limit to 6 MPa resulted in overestimating the maximum shear strain in the first half of the gait cycle.

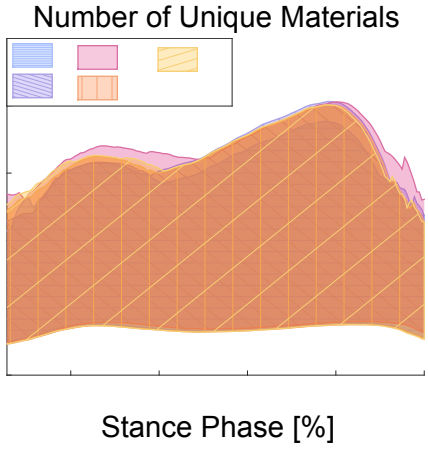

FIGURE 7 A sensitivity study of the number of materials in the T_2-refined material model showed that slightly increasing or decreasing the number of materials had a relatively small impact on the predicted maximum shear strain.

changes in $T_{1\rho}$ and T_2 relaxation times [12]. However, to our knowledge this study is the first to investigate the use of T_2 relaxation to directly refine material properties within subject-specific FE models.

For three subjects with varying KL grades, we built two FE models with subject-specific geometry; the first with T_2-refined moduli and the second with a homogeneous modulus. For all subjects, the T_2-refined material model produced significantly higher maximum 1^{st} principal stress, maximum shear strain, and cumulative stress in almost all cartilage regions. The maximum 1^{st} principal stress seen in the T_2-refined models was around 7 MPa while the maximum shear strain was just above 0.3 which is comparable to previous studies [48, 36, 43, 49, 11]. We also calculated the cumulative maximum principal stress as defined by Klets et al. [44]. The maximum cumulative stress value seen in our models was around 4 MPa which is comparable to the normal weight subjects evaluated in Klets et al. [44].

The resulting difference in predicted mechanical behavior between material models suggests that a model with T_2-refined material properties predicts higher stresses and strains, in regions of high T_2, than a model assigned with homogeneous material properties. The T_2-refined material model simulation results, specifically regional cumulative stress, correlated better with regional MOAKS scores in both baseline and follow-up time points. The significant correlation at the end-of-study time point suggests that the T_2-refined model has better predictive power than the homogeneous model. The improvement in correlation appears to be in part due to the T_2-refined model predicting higher stress within the femoral lateral central and tibial lateral anterior regions (Figure 5). This could indicate that a T_2-refined model is more sensitive to early cartilage degradation. In brief, our results suggest that a T_2-refined material model could improve simulation sensitivity to regions at risk of increased stress and strain and therefore susceptible to tissue degeneration.

The results from the sensitivity study suggest that a T_2-refined model is sensitive to changes in the range of the dynamic modulus used. Decreasing the lower limit of the dynamic modulus by 25% caused a nearly 40%

increase in the predicted maximum shear strain. However, the T_2-refined model was not highly sensitive to the number of materials used. Decreasing the number of materials by 20% caused only a 10% change in the predicted maximum shear strain. These results suggest that a T_2-refined model requires the modulus range to be appropriately defined but is not greatly affected by the number of materials. While increasing the number of materials may slightly improve model accuracy, the model accuracy is also impacted by many other factors, including the resolution of the T_2 image, the slope and range of the T_2-to-modulus conversion, and the type of material model.

Since these simulations only consisted of loads consistent with moderate walking, it was not surprising that the measured stresses did not exceed the stress-linked collagen degeneration threshold. A limitation of our work is that we do not model cartilage using a viscoelastic or biphasic response; however, previous studies have concluded that incompressible elastic response and biphasic response are nearly identical when loading occurs over a short time span, which applies to this study [34]. We also assumed all tissues to have isotropic material properties and no depth dependencies. While this assumption is simplistic, the goal of this study was to understand the impact of having T_2-refined material properties over homogeneous material properties. We were also limited by the data from the OAI which does not include MRI based measures of anisotropy, fiber orientation, or depth-dependence that are subject-specific. Overall, the presented method of using T_2 MRI to refine material properties could realistically be applied to any type of material model to improve patient-specific prediction of cartilage degeneration.

In future studies, we may further test the hypothesis that T_2-refined models improve sensitivity to early degenerative changes by comparing the sensitivity of T_2-refined and homogeneous FE models to artificial regional changes in T_2 maps. We could also test the correlation between stress or strain levels and the change in T_2 maps in subsequent follow-ups using statistical parametric mapping [50, 51].

In summary, we have developed a novel method for defining cartilage material properties from T_2 maps and demonstrated its potential to improve subject-specificity of FE models. *Clinical Impact:* T_2-refined material properties can improve subject-specific finite element model predictions of cartilage degeneration.

references

[1] J MP, AJ B, FM C, PG C, C C, MB G, et al. Osteoarthritis. Nature reviews Disease primers 2016 oct;2. https://pubmed.ncbi.nlm.nih.gov/27734845/.

[2] SR G, MB G. Changes in the osteochondral unit during osteoarthritis: structure, function and cartilage-bone crosstalk. Nature reviews Rheumatology 2016 nov;12(11):632–644. https://pubmed.ncbi.nlm.nih.gov/27652499/.

[3] KD B, RS F, EM B, B K. Radiographic grading of the severity of knee osteoarthritis: relation of the Kellgren and Lawrence grade to a grade based on joint space narrowing, and correlation with arthroscopic evidence of articular cartilage degeneration. Arthritis and rheumatism 1991;34(11):1381–1386. https://pubmed.ncbi.nlm.nih.gov/1953815/.

[4] Kijowski R, Blankenbaker Paul Stanton Jason Fine Arthur De Smet Kijowski DR, Smet DA. Arthroscopic Validation of Radiographic Grading Scales of Osteoarthritis of the Tibiofemoral Joint. American Journal of Roentgenology 2006;187:794–799. www.ajronline.org.

[5] W WR, R RJ, K HA, J HL, A GE, P AJ, et al. Osteoarthritis Classification Scales: Interobserver Reliability and Arthroscopic Correlation. The Journal of Bone and Joint Surgery;http://dx.doi.org/10.2106/JBJS.M.00929.

[6] Hunter DJ, Zhang YQ, Tu X, LaValley M, Niu JB, Amin S, et al. Change in Joint Space Width Hyaline Articular Cartilage Loss or Alteration in Meniscus? ARTHRITIS & RHEUMATISM 2006;54(8):2488–2495.

[7] Abdelaziz H, Balde OM, Citak M, Gehrke T, Magan A, Haasper C, et al. Kellgren-Lawrence scoring system underestimates cartilage damage when indicating TKA: preoperative radiograph versus intraoperative photograph. Archives of Orthopaedic and Trauma Surgery 2019;139:1287–1292. https://doi.org/10.1007/s00402-019-03223-6.

[8] Lespasio MJ, Piuzzi NS, Husni E, George M, Muschler F, Guarino AJ, et al. Knee Osteoarthritis: A Primer. The Permanente Journal/Perm J 2017;21:16–183.

[9] Mononen ME, Liukkonen MK, Korhonen RK. Utilizing Atlas-Based Modeling to Predict Knee Joint Cartilage Degeneration: Data from the Osteoarthritis Initiative. Annals of Biomedical Engineering 2019 mar;47(3):813–825.

[10] Gardiner BS, Woodhouse FG, Besier TF, Grodzinsky AJ, Lloyd DG, Zhang L, et al. Predicting Knee Osteoarthritis. Annals of Biomedical Engineering 2016 jan;44(1):222–233. https://link.springer.com/article/10.1007/s10439-015-1393-5.

[11] Bolcos PO, Mononen ME, Tanaka MS, Yang M, Suomalainen JS, Nissi MJ, et al. Identification of locations susceptible to osteoarthritis in patients with anterior cruciate ligament reconstruction: Combining knee joint computational modelling with follow-up T 1ρ and T 2 imaging. Clinical Biomechanics 2019;p. 104844. https://doi.org/10.1016/j.clinbiomech.2019.08.004.

[12] Orozco GA, Bolcos P, Mohammadi A, Tanaka MS, Yang M, Link TM, et al. Prediction of local fixed charge density loss in cartilage following ACL injury and reconstruction: A computational proof-of-concept study with MRI follow-up. Journal of Orthopaedic Research 2020;https://pubmed.ncbi.nlm.nih.gov/32639603/.

[13] Papaioannou G, Nianios G, Mitrogiannis C, Fyhrie D, Tashman S, Yang KH. Patient-specific knee joint finite element model validation with high-accuracy kinematics from biplane dynamic Roentgen stereogrammetric analysis. Journal of Biomechanics 2008 aug;41(12):2633–2638.

[14] Mononen ME, Jurvelin JS, Korhonen RK. Implementation of a gait cycle loading into healthy and meniscectomised knee joint models with fibril-reinforced articular cartilage. Computer Methods in Biomechanics and Biomedical Engineering 2015 jan;18(2):141–152. https://pubmed.ncbi.nlm.nih.gov/23570549/.

[15] Wayne JS, Kraft KA, Shields KJ, Yin C, Owen JR, Disler DG. MR Imaging of Normal and Matrix-depleted Cartilage: Correlation with Biomechanical Function and Biochemical Composition. Radiology 2003 aug;228(2):493–499. http://pubs.rsna.org/doi/10.1148/radiol.2282012012.

[16] Nieminen MT, Töyräs J, Laasanen MS, Silvennoinen J, Helminen HJ, Jurvelin JS. Prediction of biomechanical properties of articular cartilage with quantitative magnetic resonance imaging. Journal of Biomechanics 2004 mar;37(3):321–328.

[17] Kurkijärvi JE, Nissi MJ, Kiviranta I, Jurvelin JS, Nieminen MT. Delayed gadolinium-enhanced MRI of cartilage (dGEMRIC) and T2 characteristics of human knee articular cartilage: Topographical variation and relationships to mechanical properties. Magnetic Resonance in Medicine 2004;52(1):41–46. https://pubmed.ncbi.nlm.nih.gov/15236365/.

[18] DD C, CP N, ML H. Articular cartilage deformation determined in an intact tibiofemoral joint by displacement-encoded imaging. Magnetic resonance in medicine 2009;61(4):989–993. https://pubmed.ncbi.nlm.nih.gov/19189290/.

[19] DD C, L C, KD B, SB T, EA N, CP N. In vivo articular cartilage deformation: noninvasive quantification of intratissue strain during joint contact in the human knee. Scientific reports 2016 jan;6. https://pubmed.ncbi.nlm.nih.gov/26752228/.

[20] T L, E T, BR K, NP S, M Z, H M, et al. Quantification of patellofemoral cartilage deformation and contact area changes in response to static loading via high-resolution MRI with prospective motion correction. Journal of magnetic resonance imaging : JMRI 2019 nov;50(5):1561–1570. https://pubmed.ncbi.nlm.nih.gov/30903682/.

[21] Nissi MJ, Rieppo J, Töyräs J, Laasanen MS, Kiviranta I, Nieminen MT, et al. Estimation of mechanical properties of articular cartilage with MRI - dGEMRIC, T2 and T1 imaging in different species with variable stages of maturation. Osteoarthritis and Cartilage 2007 oct;15(10):1141–1148. https://pubmed.ncbi.nlm.nih.gov/17513137/.

[22] Pierce DM, Trobin W, Raya JG, Trattnig S, Bischof H, Glaser C, et al. DT-MRI Based Computation of Collagen Fiber Deformation in Human Articular Cartilage: A Feasibility Study. Annals of Biomedical Engineering;.

[23] Räsänen LP, Mononen ME, Nieminen MT, Lammentausta E, Jurvelin JS, Korhonen RK. Implementation of subject-specific collagen architecture of cartilage into a 2D computational model of a knee joint-data from the osteoarthritis initiative (OAI). Journal of Orthopaedic Research 2013 jan;31(1):10–22. https://pubmed.ncbi.nlm.nih.gov/22767415/.

[24] Räsänen LP, Tanska P, Mononen ME, Lammentausta E, Zbýň Š, Venäläinen MS, et al. Spatial variation of fixed charge density in knee joint cartilage from sodium MRI – Implication on knee joint mechanics under static loading. Journal of Biomechanics 2016 oct;49(14):3387–3396.

[25] Ishijima M, Watari T, Naito K, Kaneko H, Futami I, Yoshimura-Ishida K, et al. Relationships between biomarkers of cartilage, bone, synovial metabolism and knee pain provide insights into the origins of pain in early knee osteoarthritis. Arthritis Research and Therapy 2011 feb;13(1):1–8. https://link.springer.com/articles/10.1186/ar3246https://link.springer.com/article/10.1186/ar3246.

[26] Hunter DJ, Guermazi A, Lo GH, Grainger AJ, Conaghan PG, Boudreau RM, et al. Evolution of semi-quantitative whole joint assessment of knee OA: MOAKS (MRI Osteoarthritis Knee Score). Osteoarthritis and Cartilage 2011 aug;19(8):990–1002. https://pubmed.ncbi.nlm.nih.gov/21645627/.

[27] FW R, CK K, MJ H, DJ H, F E, Z W, et al. Can structural joint damage measured with MR imaging be used to predict knee replacement in the following year? Radiology 2015 mar;274(3):810–820. https://pubmed.ncbi.nlm.nih.gov/25279436/.

[28] FW R, CK K, MJ H, DJ H, F E, T F, et al. What comes first? Multitissue involvement leading to radiographic osteoarthritis: magnetic resonance imaging-based trajectory analysis over four years in the osteoarthritis initiative. Arthritis & rheumatology (Hoboken, NJ) 2015 aug;67(8):2085–2096. https://pubmed.ncbi.nlm.nih.gov/25940308/.

[29] Peterfy CG, Schneider E, Nevitt M, The osteoarthritis initiative: report on the design rationale for the magnetic resonance imaging protocol for the knee. W.B. Saunders Ltd; 2008. https://www.ncbi.nlm.nih.gov/pmc/articles/PMC3048821/.

[30] Rodriguez-Vila B, Sánchez-González P, Oropesa I, Gómez EJ, Pierce DM. Automated Hexahedral Meshing of Knee Cartilage Structures – Application to Data from the Osteoarthritis Initiative. Computer Methods in Biomechanics and Biomedical Engineering 2017;20:1543–1553.

[31] Maas SA, Ellis BJ, Ateshian GA, Weiss JA. FEBio: Finite elements for biomechanics. Journal of Biomechanical Engineering 2012 jan;134(1).

[32] Lampen N, Su H, Chan D, Yan P. T2 Mapping Refined Finite Element Modeling to Predict Knee Osteoarthritis Progression. In: Accepted for publication in Proceedings of the Annual International Conference of the IEEE Engineering in Medicine and Biology Society, EMBS; 2021. .

[33] MATLAB. version R2020a. Natick, Massachusetts: The MathWorks Inc.; 2020.

[34] Ateshian GA, Ellis BJ, Weiss JA. Equivalence between short-time biphasic and incompressible elastic material responses. Journal of Biomechanical Engineering 2007 jun;129(3):405–412.

[35] Waldstein W, Perino G, Gilbert SL, Maher SA, Windhager R, Boettner F. OARSI osteoarthritis cartilage histopathology assessment system: A biomechanical evaluation in the human knee. Journal of Orthopaedic Research 2016 jan;34(1):135–140. https://pubmed.ncbi.nlm.nih.gov/26250350/.

[36] Klets O, Mononen ME, Tanska P, Nieminen MT, Korhonen RK, Saarakkala S. Comparison of different material models of articular cartilage in 3D computational modeling of the knee: Data from the Osteoarthritis Initiative (OAI). Journal of Biomechanics 2016 dec;49(16):3891–3900. http://dx.doi.org/10.1016/j.jbiomech.2016.10.025.

[37] Moerman KM. GIBBON: The Geometry and Image-Based Bioengineering add-On. Journal of Open Source Software 2018 feb;3(22):506. https://joss.theoj.org/papers/10.21105/joss.00506.

[38] Westerterp KR. Pattern and intensity of physical activity. Nature 2001 mar;410(6828):539. http://www.ctlab.geo.utexas.edu/pubs/.

[39] Bergmann G, Bender A, Graichen F, Dymke J, Rohlmann A, Trepczynski A, et al. Standardized Loads Acting in Knee Implants. PLoS ONE 2014 jan;9(1):e86035. https://dx.plos.org/10.1371/journal.pone.0086035.

[40] H G, TJ S, T C, H W, C B, SL G, et al. A statistically-augmented computational platform for evaluating meniscal function. Journal of biomechanics 2015 jun;48(8):1444–1453. https://pubmed.ncbi.nlm.nih.gov/25757666/.

[41] Guo H, Santner TJ, Lerner AL, Maher SA. Reducing uncertainty when using knee-specific finite element models by assessing the effect of input parameters. Journal of Orthopaedic Research 2017 oct;35(10):2233–2242.

[42] D'lima DD, Hashimoto S, Chen PC, Colwell CW, Lotz MK. Human chondrocyte apoptosis in response to mechanical injury. Osteoarthritis and Cartilage 2001;.

[43] Mononen ME, Tanska P, Isaksson H, Korhonen RK. A novel method to simulate the progression of collagen degeneration of cartilage in the knee: Data from the osteoarthritis initiative. Scientific Reports 2016 feb;6(1):1–14.

[44] Klets O, Mononen ME, Liukkonen MK, Nevalainen MT, Nieminen MT, Saarakkala S, et al. Estimation of the Effect of Body Weight on the Development of Osteoarthritis Based on Cumulative Stresses in Cartilage: Data from the Osteoarthritis Initiative. Annals of Biomedical Engineering 2018 feb;46(2):334–344. https://pubmed.ncbi.nlm.nih.gov/29280031/.

[45] BenSaïda A, Shapiro-Wilk and Shapiro-Francia normality tests. MATLAB Central File Exchange; 2021. https://www.mathworks.com/matlabcentral/fileexchange/13964-shapiro-wilk-and-shapiro-francia-normality-tests.

[46] Carey RE, Zheng L, Aiyangar AK, Harner CD, Zhang X. Subject-specific finite element modeling of the tibiofemoral joint based on ct, magnetic resonance imaging and dynamic stereo-radiography data in vivo. Journal of Biomechanical Engineering 2014;136(4). https://pubmed.ncbi.nlm.nih.gov/24337180/.

[47] Mohammadi A, Myller KAH, Tanska P, Hirvasniemi J, Saarakkala S, Töyräs J, et al. Rapid CT-based Estimation of Articular Cartilage Biomechanics in the Knee Joint Without Cartilage Segmentation. Annals of Biomedical Engineering 2020 dec;48(12):2965–2975. https://doi.org/10.1007/s10439-020-02666-y.

[48] Mononen ME, Mikkola MT, Julkunen P, Ojala R, Nieminen MT, Jurvelin JS, et al. Effect of superficial collagen patterns and fibrillation of femoral articular cartilage on knee joint mechanics-A 3D finite element analysis. Journal of Biomechanics 2012 feb;45(3):579–587.

[49] Afsar E, Taspinar F, Calik BB, Ozkan Y, Gok K. Use of the finite element analysis to determine stresses in the knee joints of osteoarthritis patients with different Q angles. Journal of the Brazilian Society of Mechanical Sciences and Engineering 2017 apr;39(4):1061–1067. https://link.springer.com/article/10.1007/s40430-016-0636-1.

[50] Wright IC, McGuire PK, Poline JB, Travere JM, Murray RM, Frith CD, et al. A voxel-based method for the statistical analysis of gray and white matter density applied to schizophrenia. NeuroImage 1995 dec;2(4):244–252.

[51] Pedoia V, Lee J, Norman B, Link TM, Majumdar S. Diagnosing osteoarthritis from T2 maps using deep learning: an analysis of the entire Osteoarthritis Initiative baseline cohort. Osteoarthritis and Cartilage 2019 jul;27(7):1002–1010. https://doi.org/10.1016/j.joca.2019.02.800.